Origin of Carbon Nanotubes Induced Poly(L-Lactide) Crystallization: Surface Induced Conformational Order

Xiao Hu,[†] Haining An,[†] Zhong-Ming Li,*[,†] Yong Geng,[§] Liangbin Li,[‡] and Chuanlu Yang[§]

College of Polymer Science and Engineering and State Key Laboratory of Polymer Materials Engineering, Sichuan University, Chengdu, China, Department of Physics and Electrons, Ludong University, Yantai, China, and National Synchrotron Radiation Laboratory and Department of Polymer Science and Engineering, University of Science and Technology of China, Hefei, China

Received December 12, 2008
Revised Manuscript Received February 20, 2009

Introduction

Carbon nanotubes (CNTs) have been recognized as an effective nucleating agent to enhance the crystallization kinetics of polymers and induce unique crystalline morphology. The initial investigations have focused on the high nucleation efficiency of CNTs.[1,2] For example, Agarwal et al. found that CNTs can nucleate crystallization of poly(ethylene terephthalate) at concentrations as low as 0.03 wt %.[3] Recent experiments have shown that, in additional to the nucleating effect, CNTs are very efficient in templating polymer lamellae to grow perpendicular to the CNT surface in a shish-kebab fashion even under quiescent conditions.[4−6] Because of the power of CNTs as nucleating agents, shear has a minor effect on the crystallization kinetics.[4] Interestingly, Li, et al. have patterned polymeric materials periodically on individual carbon nanotubes, resulting in nanohybrid shish-kebab (NHSK) structures, where a single CNT is regarded as the shish.[7,8] These reports imply that CNTs alone can induce orientation of polymer chains even without imposition of flow (shear, elongational, or mixed flow) which is generally applied to incur formation of oriented crystals.[9−11] The indicator of oriented lamellae is the formation of fiber-like nucleation precursors (or mesophase) at an early stage of crystallization, which are oriented chain clusters or bundles above a critical size.

Unfortunately, what happens in the early stage of CNT-induced polymer crystallization is far from clear, even though it is a crucial guide to the route taken in crystallization. Up to now, more and more reports have shown that a preordering structure exists before or at the early stage of polymer crystallization. Polymer preordering comprises intermolecular positional and orientational order as well as intramolecular conformational order. Before the crystallite appears, polymer chains go through conformation adjustment and orientation transformation in a way which favors the formation of crystallites.[12−14] In this study, we attempt to reveal the origin of CNT-induced polymer crystallization at an early stage with the help of in situ Fourier transform infrared spectroscopy (FTIR).

FTIR is highly sensitive to the conformation and packing density of polymers, making it useful for probing the crystallization behavior of polymers, especially at the molecular level and at the very early stages.[14−16] Characteristic bands representing specific group vibrations can be correlated with the crystalline and amorphous fractions of the bulk. According to the shape and intensity changes of FTIR bands in the course of crystallization, chain conformational order and the subsequent crystallization behavior can be evaluated.

In this work, we chose poly(L-lactide) (PLLA), an increasingly popular biodegradable polymer, as the model polymer for these reasons: (i) PLLA crystallizes quite slowly, even if CNTs are incorporated and there is a relatively long time to nucleate, which provides the possibility of online determination of its structure;[17] (ii) pure PLLA crystallization has been extensively investigated and some of the mechanisms underlying this are widely accepted. Pre-existing research has established a valuable foundation for investigation of the PLLA nanocomposite conformation. PLLA can crystallize in α, β, or γ forms depending on the processing conditions. It forms the most common α form from the melt or solution under normal conditions, with a 10_3 helical chain conformation in which two chains interact to form an orthorhombic unit cell.[18,19] The β-form was obtained by stretching the α-form at a very high drawing ratio and at high temperature.[20] Finally, the γ-form, which can be prepared by epitaxial crystallization, was recently described by Cartier et al.[21] The formation of the α-PLLA 10_3 helix conformation is ascribed to the interchain interactions between the $-CH_3$ groups whose structural adjustment precedes that of the ester group, as recently proposed by Zhang et al.[22] Moreover, the relevant FTIR conformational vibrations of PLLA are available.[23,24] IR bands at 921, 1210, and 1456 cm^{-1} were chosen, corresponding to intrachain 10_3 helix formation, the combination of −COC and $-CH_3$ interchain interaction and $-CH_3$ interchain interaction, respectively.

Experimental Section

Materials. The PLLA (Model 5051X) used in this test is an injection grade granular material manufactured by Cargill Dow Co. (Japan). The $\bar{M}_n$ is 6.24×10^4 g·mol^{-1} and the $\bar{M}_w$ is 9.32×10^4 g·mol^{-1}. Two types of commercially available multiwall carbon nanotubes were purchased from Chengdu Organic Chemicals Co., Ltd., the Chinese Academy of Sciences R&D center for Carbon Nanotubes. One type consists of carboxyl carbon nanotubes, where some −COOH groups have been grafted on to the surface of CNTs. Detailed information for these two types of CNTs is included in Table 1.

Sample Preparation. Solution coagulation was utilized to prepare the PLLA/CNTs nanocomposites. 0.01 g CNTs were added to 20 mL methylene dichloride (CH_2Cl_2), ultrasonically mixing for 40 min. At the same time 10 g of PLLA was dissolved in 100 mL of CH_2Cl_2. By dropping the predispersed CH_2Cl_2/CNTs solution into the CH_2Cl_2/PLLA hybrid, a uniform CH_2Cl_2/PLLA/CNTs solution was obtained. Pure PLLA was also dissolved under exactly the same conditions for comparison. Solutions were poured into evaporating dishes and dried overnight at room temperature to evaporate the solvent and form membranes. The membranes were then relocated to a vacuum oven at room temperature for 24 h to

Table 1. Properties of Commercially Purchased Multi-Wall Carbon Nanotubes

	pure MWCNT	carboxyl MWCNT
length	∼20 μm	∼20 μm
outside diameter (OD)	30−50 nm	30−50 nm
purity	>95 wt %	>95 wt %
−COOH content	0	0.73 wt %
special surface area (SSA)	>60 m^2/g	>60 m^2/g

* To whom correspondence should be addressed. E-mail: zmli@scu.edu.cn.
[†] Sichuan University.
[§] Ludong University.
[‡] University of Science and Technology of China.

10.1021/ma802758k CCC: $40.75
Published on Web 04/02/2009

release solvent thoroughly. The final thicknesses were about 30 μm.

Time-Solved Fourier Transform Infrared Spectroscopy (FTIR) Characterization. In situ IR spectra were collected over the wavenumber range 800−1500 cm^{-1} using a Bruker TENSOR 37 FTIR spectrometer with a resolution of 2 cm^{-1}. A homemade parallel plate cell was employed as the hot stage. Two ZnSe plates were used as IR windows, enclosing PLLA samples. Each sample was kept at 200 °C for 10 min to completely melt any residual crystalline domains and to erase any thermal history. Then the melt was cooled to 124 °C at a rate of 10 °C/min and data collection begun. In fact, we tried several temperatures. However, extremely slow crystal growth of PLLA occurred at higher temperatures and it was impossible to differentiate any changes in the various vibrations when a lower temperature was used. Hence, 124 °C was chosen as an appropriate temperature to facilitate the crystallization of pure PLLA and the nanocomposites. The spectra were collected at 1 min intervals for CNTs samples and 2 min intervals for neat PLLA.

Results and Discussion

Figure 1 shows representative time-resolved FTIR spectra of neat PLLA (a) and PLLA/CNTs nanocomposites (b and c) during isothermal crystallization at 124 °C. The range from 1000 to 1500 cm^{-1} is mainly attributed to the asymmetric deformation mode of $-CH_3$, the bending vibration of −CH group and the C−O−C stretching band, while the backbone stretching and $-CH_3$ rocking bands are mostly distributed in the 840−960 cm^{-1} range. Intensity changes and band shifts in the FTIR spectra are highly sensitive to structural changes taking place during crystallization.[25] The intensities of the crystal-dependent bands increase while the amorphous-sensitive bands decrease as the crystallization progresses. For clearer observation, bands from 840 to 960 cm^{-1} are shown separately in Figure 1d. The band at 921 cm^{-1} is recognized as being related to crystallization. Its absence at the early stage of crystallization indicates that there are no crystallites. Then this peak becomes visible and its intensity increases until the crystallization is complete. However, at the same time, the intensities of the amorphous-dependent bands such as that at 955 cm^{-1} continue to fall. Quite noticeably, the 866 cm^{-1} band shifts to 872 cm^{-1} simultaneously with the increase of the crystallinity. Band shifts to higher wavenumbers and sharpening suggest a transition to a well-defined order.[24]

In order to compare the overall crystallization kinetics of PLLA and its CNT nanocomposites, the normalized intensity of the 921 cm^{-1} band as a function of time is illustrated in Figure 2. It presents typical sigmoidal evolution. Both the induction time, defined as the time required to detect a significant increase in conversion relative to the initial stage and $t_{1/2}$, or the time at which the crystallization reaches 50% completion, which is related to the nucleation characteristics of the system and the bulk crystallization kinetics, show the same trend. Pure CNTs are always faster than carboxyl CNTs, which are followed by neat PLLA. The PLLA/CNTs samples complete the crystallization process within a time approximately 1/10 that of neat PLLA. Also, the pure CNTs complete the crystallization process three times faster than the carboxyl CNTs. These results provide convincing evidence that CNTs are indeed excellent nucleators for PLLA. However, it is even more interesting that the carboxyl functionalization of the CNTs' surface depresses their nucleation effect. Due to the different thermodynamic driving forces for nucleation and growth, for the same thermal history, the three materials crystallize in different manners, especially with CNTs and pure CNTs composites, so there must be different nucleation mechanisms underlying the early stage of crystallization.

Three bands were studied closely. The peak heights at 1456 cm^{-1} and 1210 cm^{-1} were used to probe the conformational changes in the backbone, while the 921 cm^{-1} band was used to follow the kinetics of the 10_3 helix formation. The former reveals the interchain interaction and the latter the intrachain interaction.[25]

Figure 3 illustrates the variation of each of these three peaks over the crystallization period. As mentioned above, the absence of the 921 cm^{-1} band indicates that there are no crystallites in the melt, so the times 0−1800 s for PLLA (Figure 3a), 0−120 s for pure CNTs (Figure 3b) and 0−480 s for carboxyl CNTs (Figure 3c) are considered to be the early nucleation stages. As shown in Figure 3, there is an obvious time lag in the intensity change of the 921 cm^{-1} band with respect to that of the other two bands, which implies that the conformational change in the PLLA chains already happens before the crystallization starts. In other words, the PLLA chains initially take up a similar conformation as in the crystalline phase and then pack into the crystalline lattice. Therefore, the conformational ordering is the crucial element which determines the final kinetics and structure of the crystallites. If the normalized intensity (In) at the end of the early stage of crystallization is used for comparison, the following sequences are obtained over the early nucleation stages:

PLLA: $In_{(1456)} > In_{(1210)} \sim In_{(921)}$

Pure CNTs: $In_{(1210)} > In_{(1456)} > In_{(921)}$

Carboxyl CNTs: $In_{(1210)} > In_{(1456)} > In_{(921)}$

For neat PLLA, the bulk crystallization kinetics for CH_3 interchain interaction as indicated by the intensity of the 1456 cm^{-1} band is faster than the 10_3 helix formation, which indicates that the $-CH_3$ interchain interaction is the precondition for the formation of a stable PLLA helix structure.[22] In contrast, in the nanocomposites, the 1210 cm^{-1} band, exhibits the fastest and most sensitive response to interchain comformational ordering in the early nucleation stage and always keeps ahead over the entire crystallization period. This implies that it has a decisive role in the formation of the prepacking conformational ordering frame. Some obvious questions arise: Does the preceding emergence of 1210 cm^{-1} band accelerate the formation of the conformational ordering and the sequential crystallization? What is the origin of the 1210 cm^{-1} band? How do CNTs induce the conformational order represented by the 1210 cm^{-1} band and speed up the nucleation and crystallization rate?

The adsorption of polymers on the CNT surface through CNT-polymer interaction is a quite general phenomenon. Although the binding mechanism is not yet clear, various experiments have shown that this probably arises from both the backbone and side groups of the polymers. It has been reported using computer simulation[26] that the polymer backbone provides the strongest binding to the nanotubes rather than the side groups. At the same time, Baskaran et al.[27] attributed the adsorption of macromolecules on the carbon nanotubes to the interactions between the −CH groups of the polymers and the nanotubes. Although the intermolecular CH−π interaction is weak, the present experimental conditions where the CNT content is as low as 0.1 wt % so even with ultrasonic assistance, CNTs are not expected to interact with each other to form aggregates. Under such conditions, an initial contact between a chain and the CNT surface allows for the CH−π interaction, and successive −CH groups gradually attach themselves to the surface, leading to partial or complete chain adsorption. This indicates that the efficiency of adsorption depends on the number of −CH groups and the extent of the CNT surface available

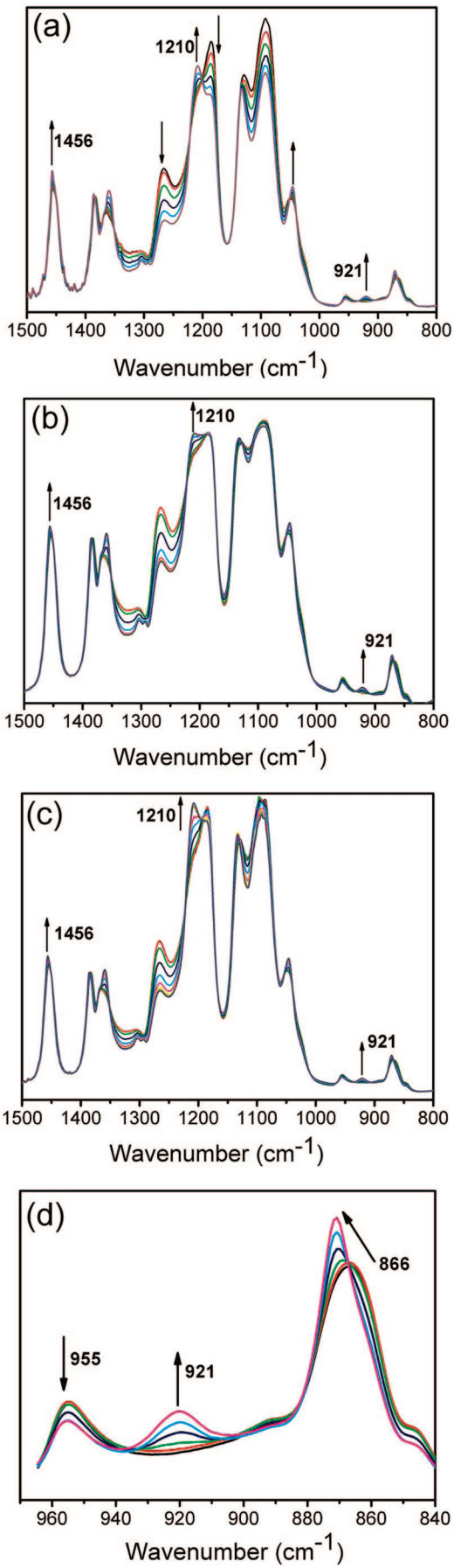

Figure 1. Time-resolved FTIR spectra for. (a) 800−1500 cm^{-1} of neat PLLA, (b) 800−1500 cm^{-1} of PLLA/pure CNTs, (c) 800−1500 cm^{-1} of PLLA/carboxyl CNTs, and (d) 840−960 cm^{-1} of neat PLLA isothermally crystallized at 124 °C.

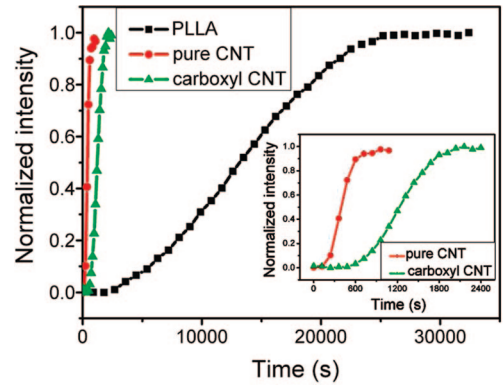

Figure 2. Normalized peak intensities at 921 cm^{-1} as a function of crystallization time for neat PLLA, pure CNTs, and carboxyl CNTs.

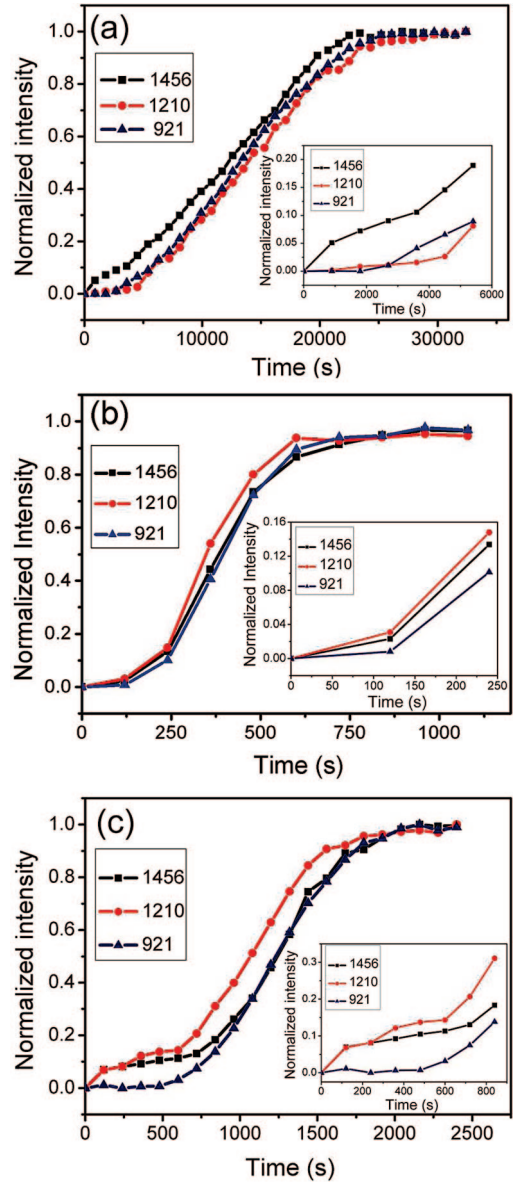

Figure 3. Normalized peak intensities at 921, 1210, and 1456 cm^{-1} as a function of crystallization time for (a) neat PLLA, (b) pure CNTs, and (c) carboxyl CNTs.

for the molecular interaction. This work has shown that it takes less time for PLLA/pure CNTs to complete crystallization than with the carboxyl CNTs, whose tube surface is partially occupied by −COOH groups. This is circumstantial evidence for

Table 2. Band Assignments of Semicrystalline PLLA[24,25]

interchain (inter)/ intrachain (intra) interaction	wavenumber (cm^{-1})	assignment
inter	1456	$\delta_{as}(CH_3)$
inter	1210	$\nu_{as}(COC) + r_{as}(CH_3)$
intra	921	backbone stretching

Scheme 1. Schematic Diagrams of Conformational Ordering in (a) PLLA and (b) PLLA/CNTs Nanocomposites

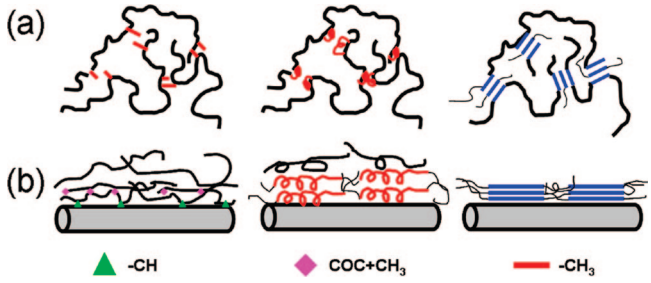

polymer−CNT wrapping through CH-π interaction, since the existence of −COOH disables the attachment of −CH groups to the CNT surface to form the CH-π interaction. Vibrational assignments for neat PLLA and PLLA/CNTs nanocomposites are shown in Table 2. The band at 1210 cm^{-1} is attributed to the combination vibration of −COC and $-CH_3$, and is assigned to an E1 mode (perpendicular to the helix axis). During crystallization, its intensity increases because the transition moments corresponding to the conformers change their orientation from a random arrangement to a in-plane orientation (formation of crystal planes).[24] The intensity increase of the 1210 cm^{-1} band in the nanocomposites indicates the unique template effect of carbon nanotubes on the conformational ordering of PLLA.

The carbon nanotube induced poly(L-lactide) crystallization is then summarized by Scheme 1. In pure PLLA, the conformational ordering begins with the interchain interaction of $-CH_3$ (labeled as a short red line). Then a short helix emerges where a couple of $-CH_3$ groups interact. Later, this short helix develops through propagation or incorporation.[14] Finally, when the helix length exceeds a certain critical value it can fold into the crystal lattice to form crystals. However, the situation is quite different for PLLA/CNTs composites. The existence of CNTs will define the landscape of the ordering of PLLA helix surrounding the PLLA/CNT interface. As explained in Scheme 1b, the surface of the CNTs induces conformational ordering through the backbone of the PLLA chains. These molecular chains adsorb the CNTs through their −CH groups and subsequent PLLA backbones make contact with the preadsorbed ones via $-(COC + CH_3)$ interactions to form a unique conformational ordering structure, which finally becomes the precursor of PLLA crystal growth and causes nucleation and overall crystallization rates to rise.

Conclusions

FTIR was employed to investigate CNT-induced PLLA crystallization, especially in the early stages. CNTs were shown to accelerate the crystallization of PLLA significantly, acting as an efficient nucleator. CNTs provide templates for the conformational ordering of PLLA by providing reactive surfaces where strong noncovalent binding with polymer main chains occurred. This kind of interaction resulted in $-(COC + CH_3)$ conformational changes that preceded equivalent changes of $-CH_3$ counterparts, causing overall assistance to the crystallization. This investigation has provided an interesting exploration of the early stages of nanocomposite crystallization.

Acknowledgment. The authors gratefully acknowledge financial support for this work by the National Natural Science Foundation of China (Contract No. 50527301). The research is also, in part, supported by the Opening Project of the State Key Laboratory of Polymer Materials Engineering, Sichuan University.

References and Notes

(1) Grady, B. P.; Pompeo, F.; Shambaugh, R. L.; Resasco, D. E. *J. Phys. Chem. B* **2002**, *106*, 5852.
(2) Bhattacharyya, A. R.; Sreekumar, T. V.; Liu, T.; Kumar, S.; Ericson, L. M.; Hauge, R. H.; Smalley, R. E. *Polymer* **2003**, *44*, 2373.
(3) Anand, K. A.; Agarwal, U. S.; Joseph, R. *Polymer* **2006**, *47*, 3976.
(4) García-Gutiérrez, M. C.; Hernández, J. J.; Nogales, A.; Panine, P.; Rueda, D. R.; Ezquerra, T. A. *Macromolecules* **2008**, *41*, 844.
(5) Mago, G.; Fisher, F. T.; Kalyon, D. M. *Macromolecules* **2008**, *41*, 8103.
(6) Haggenmueller, R.; Fischer, J. E.; Winey, K. I. *Macromolecules* **2006**, *39*, 2964.
(7) Li, L. Y.; Li, C. Y.; Ni, C. Y. *J. Am. Chem. Soc.* **2006**, *128*, 1692.
(8) Li, C. Y.; Li, L.; Cai, W.; Kodjie, S. L.; Tenneti, K. K. *Adv. Mater.* **2005**, *17*, 1198.
(9) Somani, R. H.; Hsiao, B. S.; Nogales, A.; Srinivas, S.; Tsou, A. H.; Sics, I.; Balta-Calleja, F. J.; Ezquerra, T. A. *Macromolecules* **2000**, *33*, 9385.
(10) Seki, M.; Thurman, D. W.; Oberhauser, J. P.; Kornfield, J. A. *Macromolecules* **2002**, *35*, 2583.
(11) Kumaraswamy, G.; Issaian, A. M.; Kornfield, J. A. *Macromolecules* **1999**, *32*, 7537.
(12) Fukao, K.; Miyamoto, Y. *Phys. Rev. Lett.* **1997**, *79*, 4613.
(13) Wang, Z. G.; Hsiao, B. S.; Sirota, E. B.; Agarwal, P.; Srinivas, S. *Macromolecules* **2000**, *33*, 978.
(14) An, H. N.; Zhao, B. J.; Ma, Z.; Shao, C. G.; Wang, X.; Fang, Y. P.; Li, L. B.; Li, Z. M. *Macromolecules* **2007**, *40*, 4740.
(15) Koenig, J. L. *Spectroscopy of Polymers*; American Chemical Society: Washington, DC, 1992.
(16) Chalmers, J. M.; Hannah, R. W.; Mayo, D. W. Spectra structure correlations: Polymer spectra. In *Handbook of Vibrational Spectroscopy*; Chalmers, J. M., Griffiths, P. R., Eds.; John Wiley & Sons, Ltd.: London, U.K., 2002; Vol. *4*, pp 1893−1918.
(17) Hoogsteen, W.; Postema, A. R.; Pennings, A. J.; ten Brinke, G. *Macromolecules* **1990**, *23*, 634.
(18) Desantis, P.; Kovacs, A. J. *Biopolymers* **1968**, *6*, 299.
(19) Kobayshi, J.; Asahi, T.; Ichiki, M.; Okikawa, A.; Suzuki, H.; Watanabe, T.; Fukada, E.; Shikinami, Y. *J. Appl. Phys.* **1995**, *77*, 2957.
(20) Eling, B.; Gogolewski, S.; Pennings, A. J. *Polymer* **1982**, *23*, 1587.
(21) Cartier, L.; Okihara, T.; Ikada, Y.; Tsuji, H.; Puiggali, J.; Lotz, B. *Polymer* **2000**, *41*, 8909.
(22) Zhang, J. M.; Tsuji, H.; Noda, I.; Ozaki, Y. *Macromolecules* **2004**, *37*, 6433.
(23) Zhang, J. M.; Tsuji, H.; Noda, I.; Ozaki, Y. *J. Phys. Chem. B* **2004**, *108*, 11514.
(24) Meaurio, E.; López-Rodríguez, N.; Sarasua, J. R. *Macromolecules* **2006**, *39*, 9291.
(25) Krikorian, V.; Pochan, D. J. *Macromolecules* **2005**, *38*, 6520.
(26) Panhuis, M. in het; Maiti, A.; Dalton, A. B.; van den Noort, A.; Coleman, J. N.; McCarthy, B.; Blau, W. J. *J. Phys. Chem. B* **2003**, *107*, 478.
(27) Baskaran, D.; Mays, J. W.; Bratcher, M. S. *Chem. Mater.* **2005**, *17*, 3389.

MA802758K